Sensitivity of the shortwave radiative effect of dust on particle shape: Comparison of spheres and spheroids

Päivi Haapanala,[1] Petri Räisänen,[2] Michael Kahnert,[3,4] and Timo Nousiainen[1]

Received 22 November 2011; revised 22 February 2012; accepted 23 February 2012; published 17 April 2012.

[1] The sensitivity of direct shortwave radiative effects of dust (DRE) to assumed particle shape is investigated. Radiative transfer simulations are conducted using optical properties of either spheres, mass-equivalent spheroids (mass-conserving case), or (mass-equivalent) spheroids whose number concentration is modified so that they have the same midvisible optical thickness (τ(545 nm)) as spheres (τ-conserving case). The impact of particle shape on DRE is investigated for different dust particle effective radii, optical thickness of the dust cloud, solar zenith angle, and spectral surface albedo (ocean, grass, and desert). It is found that the influence of particle shape on the DRE is strongest over ocean. It also depends very strongly on the shape distribution of spheroids used, to a degree that the results for two distributions of spheroids may deviate more from each other than from those for spheres. Finally, the effects of nonsphericity largely depend on whether the mass- or τ-conserving case is considered. For example, when using a shape distribution of spheroids recommended in a recent study for approximating the single-scattering properties of dust, the DRE at the surface differs at most 5% from that from spherical particles in the mass-conserving case. This stems from compensating nonsphericity effects on optical thickness, asymmetry parameter, and single-scattering albedo. However, in the τ-conserving case, the negative DRE at the surface can be up to 15% weaker for spheroids than spheres.

Citation: Haapanala, P., P. Räisänen, M. Kahnert, and T. Nousiainen (2012), Sensitivity of the shortwave radiative effect of dust on particle shape: Comparison of spheres and spheroids, *J. Geophys. Res.*, *117*, D08201, doi:10.1029/2011JD017216.

1. Introduction

[2] Mineral aerosol (dust) is considered to play an important role in Earth's climate system through its direct and indirect radiative effects [*Sokolik and Toon*, 1996; *Myhre and Stordal*, 2001; *Ramanathan et al.*, 2001]. However, there are still large uncertainties in the optical properties (asymmetry parameter, single scattering albedo, and optical thickness) of dust and thus also in its direct radiative effects. The uncertainties in estimating the direct radiative effects are due to our inability to determine accurately the sizes, shapes, concentrations, composition, and spatial distributions of dust particles, as well as difficulties in modeling their single-scattering properties accurately. In addition, the radiative effects depend on the external conditions such as the solar zenith angle and surface albedo.

[3] Mineral dust aerosols primarily originate from deserts and semiarid regions, and they can be transported by wind far away from the source areas [*Middleton et al.*, 2001, and references therein]. Dust particles do not have any preferential shape, but they are exclusively irregular and can also be inhomogeneous. Modeling results together with remote sensing and laboratory measurements have revealed that light scattering by dust particles differs significantly from that based on spherical model particles [*Volten et al.*, 2001; *Dubovik et al.*, 2002; *Kalashnikova et al.*, 2005; *Kahnert and Nousiainen*, 2006; *Nousiainen*, 2009; *Merikallio et al.*, 2011]. In addition, *Kahnert et al.* [2007] concluded that the use of spherical model particles can introduce substantial errors to modeled radiative effects of dust. However, in radiative transfer simulations and remote sensing applications these particles are still often described as spheres. On the basis of a number of studies [*Mishchenko et al.*, 1997; *Nousiainen and Vermeulen*, 2003; *Kahnert and Kylling*, 2004; *Nousiainen et al.*, 2006; *Dubovik et al.*, 2006; *Merikallio et al.*, 2011] model particles as simple as spheroids can reproduce the optical properties of dust-like aerosols significantly better than spheres. Spheroids are a simple model shape whose geometry is characterized by the size and aspect ratio, thus introducing only one additional parameter as compared to homogeneous spheres. In addition, whenever nonspherical model particles are used, the measure of size (size equivalence) needs to be established. The modeling of direct radiative

[1]Department of Physics, University of Helsinki, Helsinki, Finland.
[2]Climate Change Research, Finnish Meteorological Institute, Helsinki, Finland.
[3]Research Department, Swedish Meteorological and Hydrological Institute, Norrköping, Sweden.
[4]Department of Earth and Space Science, Chalmers University of Technology, Gothenburg, Sweden.

0148-0227/12/2011JD017216

effects of dust by using spheroids has been investigated by *Kahnert et al.* [2005] and *Otto et al.* [2011]. For example, *Otto et al.* [2011] studied the importance of realistic size equivalence and shape of spheroidal Saharan dust particles on optical properties and further on radiative effect of dust during one campaign day in Morocco. *Kahnert et al.* [2005] compared modeled net radiative fluxes of feldspar aerosols (at one wavelength) based on laboratory-measured phase functions to those based on spherical and spheroidal model particles. They found that the use of spheroids caused considerably smaller errors than the use of spheres. *Merikallio et al.* [2011] showed that a shape distribution that gives more weight to the aspect ratios that deviate strongly from spheres describes the laboratory measured single-scattering properties of dust better than the often used equiprobable shape distribution. Especially, the asymmetry parameter of dust can be described better with this kind of distribution than with the often used equiprobable distribution of spheroids [*Merikallio et al.*, 2011]. Such a shape distribution would be useful for investigating the radiative effect of dust.

[4] In this study, we investigate how much the choice of a size equivalence and shape distribution of spheroids may impact the radiative effects of dust. To this end, we compare radiative transfer simulations based on optical properties of spheres and shape distributions of spheroidal dust particles. Two different shape distributions of spheroids are considered: the equiprobable and the one suggested by *Merikallio et al.* [2011]. Broadband shortwave radiative transfer simulations are used to investigate how the radiative effects differ for spherical and spheroidal dust particles. In the simulations, the properties of dust (size distribution and optical thickness) and external conditions such as the solar zenith angle and surface albedo have been varied. The spheres and spheroids are compared by conserving either the mass or by modifying the number concentration so that the optical thickness of the dust cloud is conserved at one wavelength. The optical properties of dust are obtained from a database by *Dubovik et al.* [2006]. The database contains precomputed single scattering properties of polydisperse randomly oriented homogeneous spheroids that have been computed using the numerically exact *T* matrix method for small particles [*Mishchenko and Travis*, 1994], and a modified geometric optics approximation for large size parameters [*Yang and Liou*, 1996]. We note that the latter method is not exact and may thus introduce some error. However, according to *Yang et al.* [2007], the asymmetry parameters it provides agree well with those obtained from an exact method. Thus, especially considering that only relatively small portion of total extinction cross section is based on this approximate method, the overall accuracy of the database should be well suited for the present study.

[5] The paper is organized as follows. In section 2, the size-shape distributions used are briefly described. Section 3 presents an overview of how the optical properties (the asymmetry parameter, single-scattering albedo, and optical thickness) of the size-shape distributions are obtained from the database. The radiative transfer model is introduced in section 4. The modeled atmospheric absorption and the shortwave fluxes, as well as their sensitivity to the assumed size-shape distribution of dust, are illustrated in section 5, followed by the conclusions in section 6.

2. Size and Shape Distributions of Dust

[6] The shape of a spheroid can be expressed by the shape parameter:

$$\xi = \begin{cases} b/a - 1 & a \le b\,(\text{oblate}) \\ 1 - a/b & a > b\,(\text{prolate}) \end{cases}, \tag{1}$$

where a is the diameter of the spheroids along its main symmetry axis, and b the maximum diameter in the orthogonal direction. Here values for ξ vary from -1.8 to 1.8 with increment of 0.2, resulting altogether in 19 different shapes including the special case of a sphere, nine oblates, and nine prolates. In this study, the shape distributions $f(\xi,n)$ are parametrized according to

$$f(\xi, n) = C*|\xi^n|, \tag{2}$$

where C is a normalization coefficient such that the integral over all considered ξ equals unity, and n is a free parameter that defines the form of the shape distribution. Here we consider three such shape distributions: one consists solely of spheres (ξ = 0), and the other two include spheroids with either equal weights (hereafter, n = 0 distribution) or more weight to the oblates and prolates that deviate most from the sphere (hereafter, n = 3 distribution). These distributions are illustrated in Figure 1. The latter is suggested by *Merikallio et al.* [2011] to be used in climate modeling because comparisons with measurements indicate that the n = 3 distribution gives the overall best representation of the asymmetry parameter of mineral dust particles considered in their study. It is emphasized that this statement refers to the dust optical properties; it is not implied that the n = 3 distribution would describe properly the aspect ratio distribution of real dust particles. Indeed, observed aspect ratio distributions appear to be clearly different [e.g., *Wiegner et al.*, 2009]. However, real dust particles are neither spheres nor spheroids, and the shape distribution of spheroids that provides the best reproduction of the dust particles' optical properties do not necessarily resemble the dust particles' aspect ratio distribution. Indeed, *Nousiainen et al.* [2011] show that a shape distribution of spheroids that best reproduces the optical properties of a particle may not represent in any way its shape.

[7] The size distribution is assumed to be lognormal with a geometric standard deviation of σ = 2.0 as assumed in the ECHAM-HAM aerosol model for coarse-mode dust particles [*Stier et al.*, 2005]. Altogether 13 size distributions are produced by varying the effective radius, r_{eff}, of dust from 1.0 to 4.0 μm in steps of 0.25 μm. From these effective radii, r_{eff} = 1.5 μm is chosen to represent a background dust case and r_{eff} = 4 μm a dust storm case. The size distributions used cover particle radii from 0.1 to 19 μm.

3. Optical Properties of Dust

[8] In the radiative transfer simulations the dust is described by vertical profiles of ensemble-averaged asymmetry parameter, g, single-scattering albedo, ω, and layer values of optical thickness. The optical thickness, τ, depends

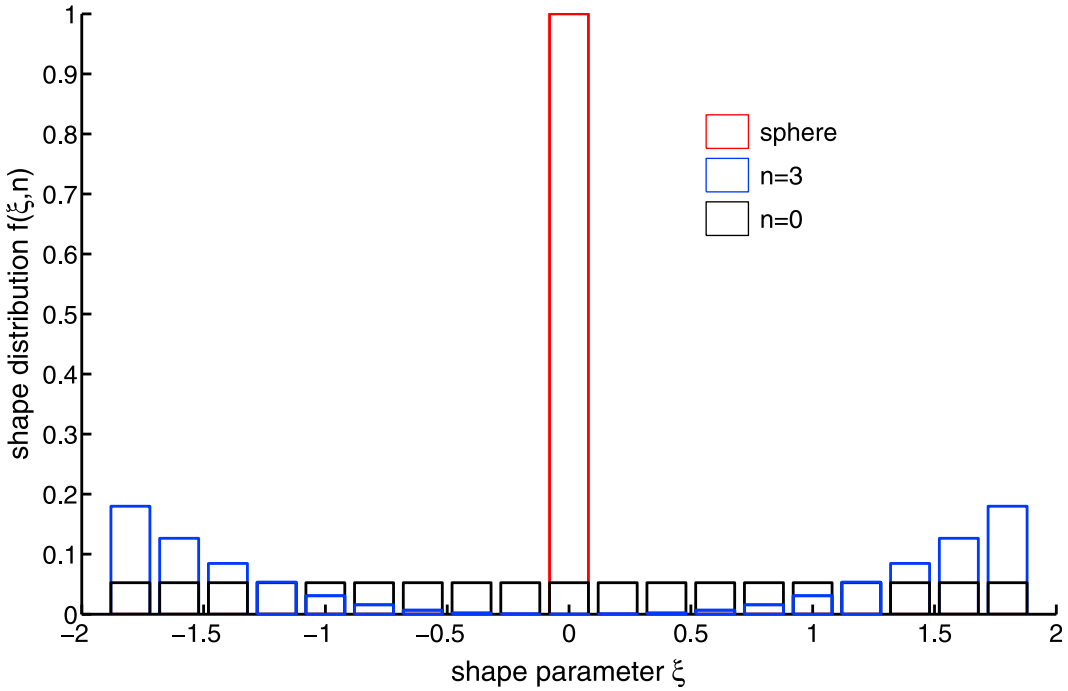

Figure 1. Weights for the three shape distributions (sphere, n = 3, and n = 0) as a function of shape parameter ξ. Shape distributions are normalized such that the integral over all ξ equals unity.

on the number concentration of the particles as well as their extinction cross section, C_{ext}, which further depends on the particle shape. Equal mass for spherical and nonspherical particles (mass-conserving case) will lead to different C_{ext} values and consequently to different optical thicknesses. However, in some cases, e.g., when the optical thickness is available from remote sensing data, it is more meaningful to conserve the optical thickness rather than the total mass. We thus also consider a case where we modify the number concentration of spheroids so that τ at a reference wavelength λ = 545 nm is the same for spherical and spheroidal dust particles. For simplicity, we call this a τ-conserving case, although, strictly speaking, τ for spheres and spheroids coincide only at the reference wavelength. Fully coincident τ values would require altering the number concentration of spheroids differently at different λ which is not realistic.

[9] To obtain the size- and shape-integrated optical properties (g, ω, and C_{ext}) of the studied size-shape distributions at several wavelengths, the database by *Dubovik et al.* [2006] was used. The frontend of the database required information about the size distribution (r_{eff}, σ), integration range (r_{min}, r_{max}), the shape distribution (weights for all shapes), and the wavelengths with corresponding refractive indices. The 23 wavelength bands covering the wavelength

Table 1. The Wavelength Bands (λ_{min} and λ_{max}) and the Corresponding Real and Imaginary Parts of the Refractive Index (Re(m) and Im(m)) of Dust[a]

	Band											
	1	2	3	4	5	6	7	8	9	10	11	12
λ_{min}	0.28	0.30	0.33	0.36	0.40	0.44	0.48	0.52	0.57	0.64	0.69	0.75
λ_{mean}	0.290	0.315	0.345	0.380	0.420	0.460	0.500	0.545	0.605	0.665	0.720	0.765
λ_{max}	0.30	0.33	0.36	0.40	0.44	0.48	0.52	0.57	0.64	0.69	0.75	0.78
Re(m)	1.519	1.528	1.527	1.516	1.512	1.515	1.516	1.517	1.517	1.517	1.517	1.518
Im(m)	0.0207	0.0185	0.0165	0.0025	0.0015	0.0013	0.0012	0.0011	0.0010	0.0010	0.0009	0.0009
	Band											
	13	14	15	16	17	18	19	20	21	22	23	
λ_{min}	0.78	0.87	1.00	1.10	1.24	1.53	1.64	2.13	2.38	2.91	3.42	
λ_{mean}	0.825	0.935	1.050	1.145	1.264	1.585	1.885	2.255	2.645	3.165	3.710	
λ_{max}	0.87	1.00	1.10	1.19	1.41	1.64	2.13	2.38	2.91	3.42	4.00	
Re(m)	1.518	1.519	1.519	1.519	1.519	1.518	1.518	1.518	1.518	1.518	1.518	
Im(m)	0.0008	0.0008	0.0007	0.0006	0.0007	0.0008	0.0011	0.0020	0.0054	0.0151	0.0389	

[a]Wavelength is in units of μm.

Table 2. The Solar Zenith Angles (SZA) and Corresponding Local Time at 20°N Latitude on 5 October

	Local Time					
	06:30	07:30	08:30	09:30	10:30	11:30
SZA (deg)	82.99	68.92	55.11	41.80	29.75	21.31

range from 0.28 to 4 μm used in this study are shown in Table 1 with the corresponding refractive indices. The wavelength bands are the same as used by the ECHAM-HAM climate model, expect for band 17, which is combined from two original bands. The refractive index of dust is also adapted from the HAM model and is based on the work by *Sokolik and Toon* [1999] and *Kinne et al.* [2003].

[10] In the radiative transfer simulations, the dust cloud is assumed to extend from the ground up to 3.0 km, and is divided into 15 vertical layers with a constant thickness of 0.2 km. Real atmospheric aerosol distributions are vertically inhomogeneous, but here, for simplicity, the dust cloud is assumed to be vertically and horizontally homogeneous, so that each layer has the same ensemble-averaged asymmetry parameter, single-scattering albedo and optical thickness.

[11] To define the optical thickness of the entire dust cloud, τ of spherical particles at the reference wavelength of λ = 545 nm ($\tau_{\mathrm{sph}}(545)$) is first assigned. Four values of $\tau_{\mathrm{sph}}(545)$ are considered: $\tau_{\mathrm{sph}} = 0.1$, $\tau_{\mathrm{sph}} = 0.3$, $\tau_{\mathrm{sph}} = 1.0$, and $\tau_{\mathrm{sph}} = 3.0$. The two smallest values are taken to describe background dust conditions, while the two largest values are more representative of dust storms.

[12] In the mass-conserving case, the optical thickness for other wavelengths and shape distributions is defined as

$$\tau_{f(\xi,n)}(\lambda) = \frac{C_{\mathrm{ext},f(\xi,n)}(\lambda)}{C_{\mathrm{ext,sph}}(545\,\mathrm{nm})} \times \tau_{sph}(545\,\mathrm{nm}), \tag{3}$$

where the $C_{\mathrm{ext,f}(\xi,\mathrm{n})}(\lambda)$ and $C_{\mathrm{ext,sph}}(545\ \mathrm{nm})$ are the extinction cross sections of a given size-shape distribution f(ξ,n) (sphere, $n = 0$ or $n = 3$) and spheres, respectively. For the τ-conserving (otc) case, the optical thickness based on spheroids is determined to match τ_{sph} at the reference wavelength of 545 nm:

$$\tau_{f(\xi,n),\,\mathrm{otc}}(\lambda) = \frac{C_{\mathrm{ext},f(\xi,n)}(\lambda)}{C_{\mathrm{ext},f(\xi,n)}(545\,\mathrm{nm})} \times \tau_{sph}(545\,\mathrm{nm}), \tag{4}$$

where the subscript $f(\xi,n)$ refers now to either $n = 0$ or $n = 3$ size-shape distribution of spheroids. Note that the assumed size and shape distributions of the particles (and therefore, their asymmetry parameter and single-scattering albedo) are the same as in the mass-conserving case; thus a different optical thickness implies a different number concentration. Altogether, for both distributions of spheroids, eight alternative wavelength-dependent layer values of optical thickness are actually used.

4. Radiative Transfer Model

[13] The libRadtran radiative transfer package [*Mayer and Kylling*, 2005] is used to simulate the shortwave (SW) radiative fluxes for both clear and dusty atmospheres. As a radiative transfer solver, the discrete ordinate radiative transfer model (DISORT) by *Stamnes et al.* [1988] is used. For wavelength bands below 780 nm, 0.5 or 1 nm wavelength resolution is used. Above 780 nm, a band parametrization by *Kato et al.* [1999] is applied. For molecular scattering and absorption we use the tropical model atmosphere by *Anderson et al.* [1986], except that the water vapor content is halved to roughly account for the dry conditions typically prevailing in regions with abundant mineral dust. Comparison with authentic tropical and midlatitude profiles by *Anderson et al.* [1986] showed that the choice of the atmosphere profile has only a very small impact on the modeled dust radiative effect.

4.1. Input Parameters

[14] The dust cloud is described with layer values of ensemble averaged optical properties (τ, ω, and g) at 23 wavelengths. In addition, the day of the year, solar zenith angle (SZA), and wavelength-dependent surface albedos are used as input. Day of the year, which determines the amount of incoming solar radiation, is chosen to be 5 October, so that the incoming solar radiation corresponds to the annual global mean value of 1365 W m^{-2}. To obtain diurnally averaged radiative fluxes, radiative transfer simulations were conducted with six solar zenith angles corresponding to local times from 06:30 to 11:30 at 20°N latitude (Table 2). Diurnally averaged fluxes are obtained as an average of the simulated daytime fluxes divided by two.

[15] The impact of particle shape on the shortwave fluxes is studied over three different surfaces (desert, ocean, and grass) over which dust plumes occur. The surface albedos for these surfaces are shown in Figure 2 as a function of wavelength. The desert (arid soil gypsiorthid) and grass (green grass) values are obtained from NASA's Advanced Spaceborne Thermal Emission Reflection Radiometer (ASTER) spectral library [*Baldridge et al.*, 2009], while for ocean, a wavelength-independent constant albedo 0.07 is used as, e.g., in the ECHAM5 model [*Roeckner et al.*, 2003]. With our wavelength bands the surface albedo for desert varies from 0.03 to 0.56 and for grass from 0.01 to 0.52.

4.2. Output Parameters

[16] The output of the radiative transfer model includes the SW direct and diffuse downward, and diffuse upward fluxes ($F^{\downarrow}_{\mathrm{dir}}$, $F^{\downarrow}_{\mathrm{diff}}$, and $F^{\uparrow}_{\mathrm{diff}}$, respectively) at the surface (z_0) and at the top of the atmosphere (TOA). The difference between the SW net fluxes ($F^{\mathrm{net}} = F^{\downarrow}_{\mathrm{dir}} + F^{\downarrow}_{\mathrm{diff}} - F^{\uparrow}_{\mathrm{diff}}$) of dusty and dust-free atmospheres is called the SW direct radiative effect of dust (DRE). At the surface, the dust radiative effect is

$$\mathrm{DRE}_{z_0} = \left(F^{net}_{z_0}\right)_{\mathrm{dusty}} - \left(F^{net}_{z_0}\right)_{\mathrm{clear\ sky}}. \tag{5}$$

At the TOA, where $F^{\downarrow}_{\mathrm{diff}}$ is always zero and $F^{\downarrow}_{\mathrm{dir}}$ is the same for both clear and dusty skies, the SW direct radiative effect of dust simplifies to the difference between clear and dusty sky diffuse upward fluxes:

$$\mathrm{DRE}_{\mathrm{TOA}} = \left(-F^{\uparrow}_{diff}\right)_{\mathrm{dusty}} - \left(-F^{\uparrow}_{diff}\right)_{\mathrm{clear\ sky}}. \tag{6}$$

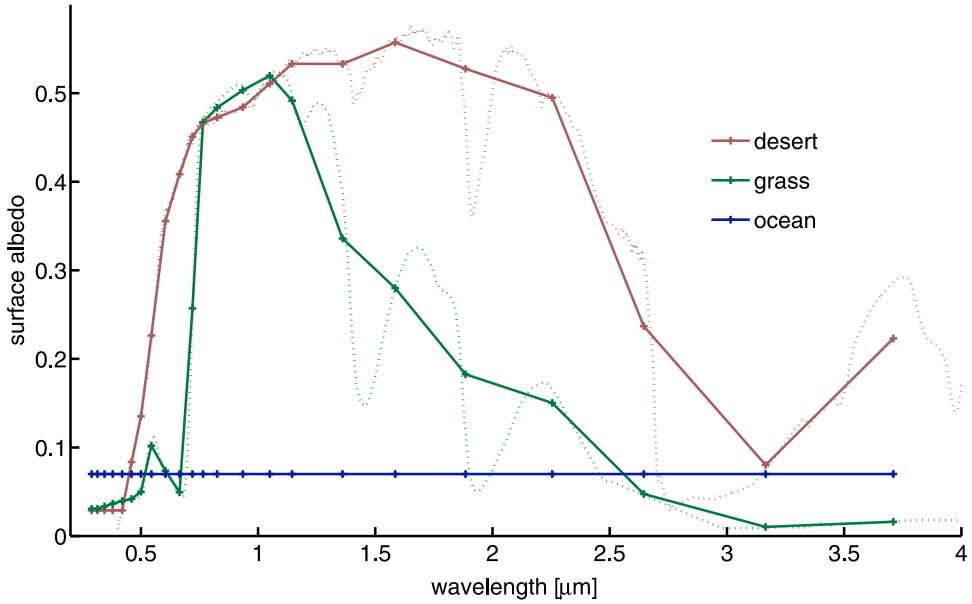

Figure 2. Surface albedos for desert (brown lines), grass (green lines), and ocean (blue lines) as a function of wavelength. The dotted lines show the original values [*Baldridge et al.*, 2009] of arid soil Gypsiorthid (desert) and green grass (grass), respectively, and the solid lines show the values used in this investigation (mean value of each of the wavelength bands).

The direct radiative effect of dust on the atmospheric absorption is defined as follows:

$$\mathrm{DRE_{ABS}} = \left[F^{\mathrm{net}}_{\mathrm{TOA}} - F^{\mathrm{net}}_{z_0}\right]_{\mathrm{dusty}} - \left[F^{\mathrm{net}}_{\mathrm{TOA}} - F^{\mathrm{net}}_{z_0}\right]_{\mathrm{clear\ sky}} = \Delta F^{\mathrm{net}}_{\mathrm{TOA}} - \Delta F^{net}_{z_0}. \quad (7)$$

Positive (negative) DRE at the TOA indicates warming (cooling) of the surface-atmosphere system as a whole. The DRE at the surface is always negative (implying surface cooling) but the DRE on atmospheric absorption is generally positive, which implies that dust increases the atmospheric radiative heating.

5. Results and Discussion

[17] Because of the large number of different parameter combinations studied (shape distributions, optical thicknesses, wavelengths, solar zenith angles, and surface albedos) most of the results are shown only for the background ($r_{\mathrm{eff}} = 1.5$ μm) and dust event ($r_{\mathrm{eff}} = 4$ μm) cases. Optical thicknesses based on $\tau_{\mathrm{sph}} = 0.1$ and $\tau_{\mathrm{sph}} = 0.3$ are used for the background case and $\tau_{\mathrm{sph}} = 1.0$ and $\tau_{\mathrm{sph}} = 3.0$ for the dust event case.

5.1. Dust Optical Properties

[18] The optical properties (τ, ω, and g) of size-shape distributions of dust are shown in Figure 3 as a function of λ and r_{eff}. Figure 3 (top) shows the τ, ω, and g values based on spherical model particles. As a general feature, the optical thickness peaks when the effective size parameter ($x_{eff} = 2\pi r_{\mathrm{eff}}/\lambda$) is near 7. Note that here the optical thickness of each size distribution of spheres is fixed at unity ($\tau_{\mathrm{sph}} = 1.0$) at the 545 nm wavelength (equation (3)). The largest values of ω are found around λ = 1500 nm and they decrease with increasing r_{eff}, which indicates increased absorption. The g values are the largest at the shortest wavelengths and they increase with increasing r_{eff}. Both the decrease in ω and increase in g with increasing r_{eff} are expected effects of increasing particle size. Figures 3 (middle) and 3 (bottom) show the impact of shape on the optical properties, that is, the difference between τ, ω, and g based on the $n = 3$ distributions of spheroids and spheres (Figure 3, middle) and the $n = 0$ distributions of spheroids and spheres (Figure 3, bottom). For spheroids, mass-conserving case is adopted and thus the optical thickness varies solely according to their respective C_{ext} values. Were the τ-conserving case used instead, all three τ would coincide at 545 nm wavelength and the values of τ based on spheroids could be up to 17% smaller than in the mass-conserving case.

[19] For distributions of spheroids, the optical thickness is nearly always larger than that for spheres, in particular for the $n = 3$ distribution for which the difference to spheres can be up to 19% in the mass-conserving case. This is expected because the area-to-mass ratio is larger for spheroids than spheres. The values of single-scattering albedo are also larger for spheroids than spheres, indicating weaker absorption, but the differences are rather small. Again the $n = 3$ distribution deviates more from spheres than the $n = 0$ distribution. The values of asymmetry parameter for the $n = 3$ distribution of spheroids are almost uniformly larger than those for spheres, with differences up to 0.05. For the $n = 0$ distribution, however, g can be either larger or smaller than for spheres. The larger the r_{eff} value, the wider is the wavelength range for which the $n = 0$ distribution produces the smallest values of g (negative values in the bottom right panel in Figure 3). In the background case ($r_{\mathrm{eff}} = 1.5$ μm) the largest relative shape impacts occur at short wavelengths (for τ around 600 nm; ω at 290 nm; g around

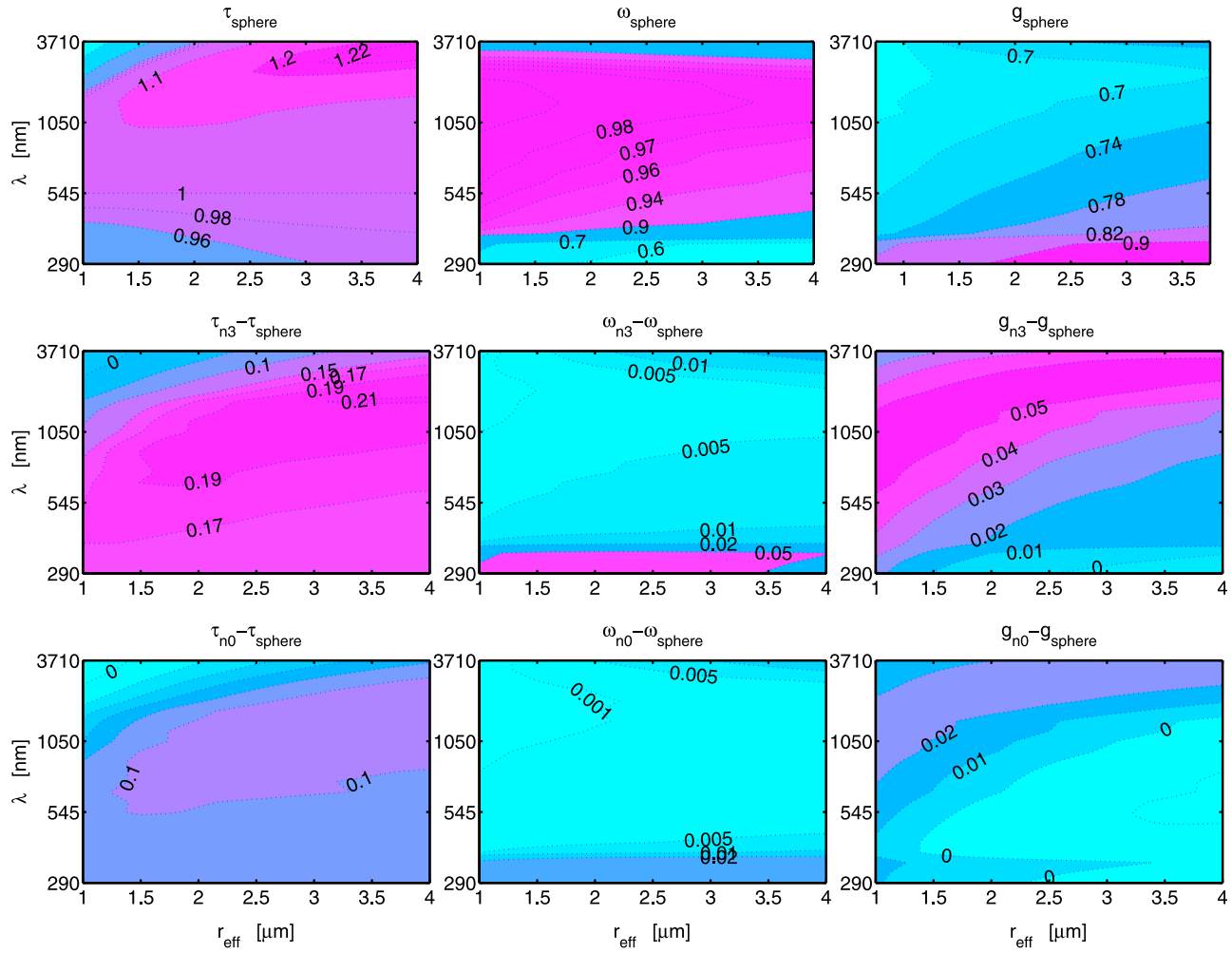

Figure 3. (top) The optical thickness (τ, τ_{sph} = 1.0), single-scattering albedo (ω), and asymmetry parameter (g) for spherical dust particles and the differences between (middle) τ, ω, and g of n = 3 distribution of spheroids and (bottom) spheres and n = 0 distribution of spheroids and spheres as a function of wavelength (λ) and size distribution (effective radius, r_{eff}). For spheroids, the mass-conserving case is adopted.

1200 nm), but they tend to move toward longer wavelengths when r_{eff} increases.

[20] Figure 3 shows that spheres and the two shape distributions of spheroids produce very similar values of ω. This agrees well with earlier studies based on spheroids [*Mishchenko et al.*, 1997; *Kahnert et al.*, 2002], circular cylinders [*Mishchenko et al.*, 1996; *Kahnert et al.*, 2002], and polyhedral prisms [*Kahnert et al.*, 2002], in which ω was found to be quite insensitive to particle shape. Note, however, that realistic dust particles can have complex morphological properties that are not accounted for by spheroids and other model particles with smooth boundary surfaces. For instance, small-scale surface roughness is a morphological feature that, for optically hard or highly absorbing particles, can significantly modulate the single scattering albedo [*Kahnert and Rother*, 2011]. However, this effect has been found to be much less pronounced for silicate aerosols with small-scale surface roughness [*Kahnert et al.*, 2012] or with a dusting of subwavelength-sized grains [*Mishchenko et al.*, 2011].

5.2. Radiative Fluxes

5.2.1. Mass-Conserving Case

[21] Let us first consider the sensitivity of the simulated, diurnally averaged SW fluxes to the dust particle shape in the mass-conserving case. Figures 4, 5, and 6 show DRE_{TOA}, DRE_{z_0}, and DRE_{ABS} as a function of r_{eff}. The rows and columns correspond to different surfaces and dust optical thicknesses (τ_{sph} = 0.1 or 3.0), respectively, and different lines correspond to the shape distributions considered. The values of shape impacts and relative shape impacts (i.e., the absolute and fractional differences in dust radiative effects based on distributions of spheroids and spheres) over ocean and desert surfaces in the background and dust storm cases are listed in Table 3. Results over a grass surface are not listed because they tend to fall between those over ocean and desert surfaces.

[22] Even though the focus of this study is to describe how the radiative effects based on nonspherical and spherical dust particles differ from each other, it is worthwhile also to describe the common features of the radiative effects of dust itself. As can be seen from Figures 4, 5, and 6, increasing r_{eff} decreases the negative radiative effect (cooling) at the TOA,

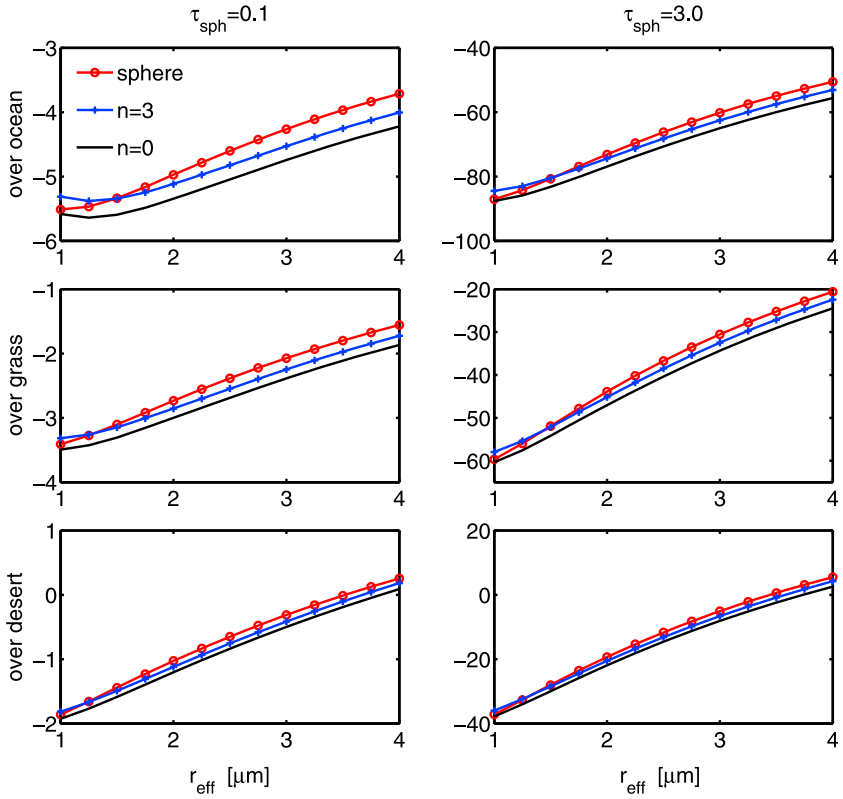

Figure 4. Diurnally averaged direct radiative effects of dust at the TOA (DRE_{TOA}) in W m^{-2} as a function of r_{eff} in the case of two optical thicknesses of dust (τ_{sph} = 0.1 and τ_{sph} = 3.0). Different lines correspond to different shape distributions. Results are shown for (top) ocean, (middle) grass, and (bottom) desert surfaces. For spheroids, the mass-conserving case is adopted.

but strengthens it at the surface. This occurs because atmospheric absorption (warming) increases substantially with increasing r_{eff} (see equation (7)). The largest absolute values of radiative effects are obtained over ocean and the smallest ones over desert. Regardless of the type of the underlying surface, the effects are stronger for optically thicker dust layers. For example, the absolute values of diurnal mean radiative effects of spherical dust particles at the TOA and the surface are always less than 25 W m^{-2} in the background cases (and less than 10 W m^{-2} in the τ_{sph} = 0.1 cases shown in Figures 4 and 5) but reach up to 50 W m^{-2} at the TOA and up to 150 W m^{-2} at the surface in the dust storm cases.

[23] Largest absolute values of shape impacts are generally obtained at the surface. In absolute terms, the shape impacts are strongest over ocean and weakest over desert, and especially the shape impacts on DRE_{z_0} tend to increase with increasing r_{eff}. Also, as expected, the differences increase with increasing optical thickness. Figures 3 and 4 show that the absolute value of shape impact on DRE_{TOA} and DRE_{z_0} tends to be larger for the n = 0 distribution. This is surprising because the single-scattering properties (Figure 2) show much smaller differences between the n = 0 distribution and spheres than between the n = 3 distribution and spheres. Actually, the larger shape impacts of the n = 3 distributions on optical properties are the reason for the smaller absolute values of shape impacts on DRE: the effect of larger optical thickness and larger asymmetry parameter partly compensate each other. Spheroids with the n = 0 distribution always produce a stronger negative DRE_{TOA} and DRE_{z_0} than spheres do. On the other hand, the DRE_{TOA} and DRE_{z_0} curves for the n = 3 distribution intersect with those for spheres, typically between r_{eff} = 1.25 μm and r_{eff} = 1.75 μm. For particles larger than that, the dust radiative effect for the n = 3 spheroids are more strongly negative than those for spheres, but not as strong as those for the n = 0 shape distribution. For the smallest values of r_{eff} however, DRE_{TOA} and DRE_{z_0} for the n = 3 distribution are weaker (less negative) than those for spheres. Thus, for shape distributions with small effective radius, the shape impact can be either negative or positive, depending on the choice of the shape distribution of spheroids. For example, the shape impacts vary from −0.8 to +0.1 W m^{-2} in the background cases and from −7.8 to −0.5 W m^{-2} in the dust storm cases (Table 3). The relative shape impacts are also larger in the dust storm cases than in the background cases, but even in the dust storm cases, they are less than 7% at the surface. The values of relative shape impacts at the TOA are, however, somewhat larger even in the case of a low-albedo ocean surface and can reach 12%. In dust storm cases over a desert surface, the relative shape impact at the TOA can be very large (up to −53%); however, this is fortuitous as DRE_{TOA} of spherical dust particles is very small in these cases.

[24] For the shape impacts on atmospheric absorption (Figure 6), the differences between spheroids and spheres are minimal for small values of r_{eff}, while for large r_{eff} (e.g., dust storm conditions), absorption is slightly larger for spheroids

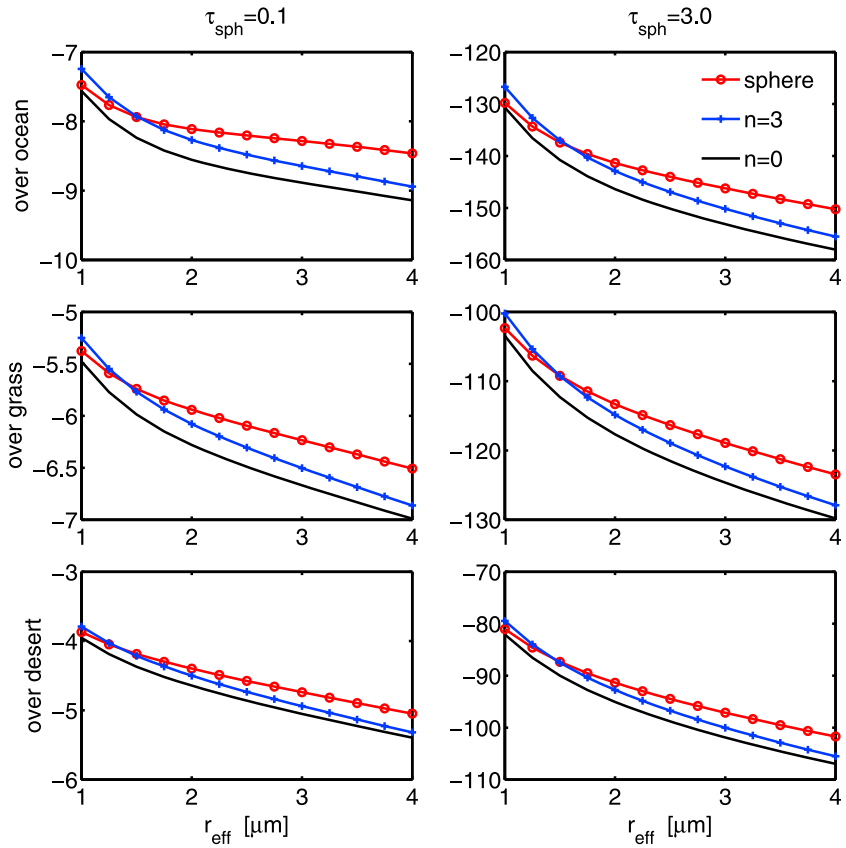

Figure 5. Same as Figure 4 but for the diurnally averaged radiative effects of dust at the surface (DRE_{z_0}). Units are W m^{-2}.

than spheres. Even in the dust storm cases the maximum absolute and relative shape impacts on DRE_{abs} (obtained with the $n = 3$ distribution) are less than +2.8 W m^{-2} and 4% (Table 3). These rather small differences reflect a compensation between the larger optical thickness and larger single-scattering albedo of mass-conserving spheroids as compared with spheres (Figure 3).

5.2.2. The τ-Conserving Case

[25] Diurnally averaged direct radiative effects of dust (DRE_{z_0}, DRE_{TOA}, DRE_{ABS}) over ocean, in the τ-conserving case, are shown in Figure 7 as a function of r_{eff}. The shape impacts over other surfaces than ocean are not shown because the surface albedo dependence of the results is quite similar to the mass-conserving cases (Figures 4, 5, and 6). Here we remind the reader that in this case, τ for spheres and spheroids coincide, but only at $\lambda = 545$ nm. By comparing Figure 7 to Figures 4 (top), 5 (top), and 6 (top), it is noted that the absolute values of radiative effects based on τ-conserving spheroids are smaller than those based on the mass-conserving ones. Consequently, both distributions of spheroids produce consistently weaker radiative effects than spheres, except at the TOA, where results based on the $n = 0$ distribution and spheres intersect. Thus, with larger r_{eff} (exact value depending on τ and surface albedo) the shape impact at the TOA can be either negative or positive depending on the shape distribution of spheroids adopted. In addition, in the τ-conserving case the maximum absolute values of shape impacts are larger, but they often have a different sign than in the mass-conserving case and they occur with the $n = 3$ distribution of spheroids. In the τ-conserving case, the shape impacts are more dominated by the differences in g and ω since the differences in optical thicknesses of spheroids and spheres are much smaller than in the mass-conserving case.

[26] The absolute and relative shape impacts over ocean and desert surfaces are listed for background and dust event cases in Table 4. The most distinct difference to the corresponding results for the mass-conserving case (in Table 3) is that in the τ-conserving case, the relative shape impacts on DRE_{z_0} and DRE_{ABS} are consistently negative. In other words, the effect of dust on the net flux at the surface and on atmospheric absorption is weaker for spheroids than spheres. This occurs because for spheroids, the ensemble-averaged single-scattering albedo is slightly higher than that for spheres, and because for the $n = 3$ distribution, also the asymmetry parameter is larger (Figure 2). Furthermore, in contrast to the mass-conserving case, the differences to spheres are in most cases more pronounced for the $n = 3$ distribution than for the $n = 0$ distribution. In particular, in the background cases, the effect of dust on the net flux at the surface and on atmospheric absorption is about 15% smaller for the $n = 3$ spheroids than for spheres, and for $\tau_{sph} = 0.3$, the absolute difference in the net flux at the ocean surface reaches +3.1 W m^{-2}. The relative shape impacts on DRE_{z_0} and DRE_{ABS} are slightly weaker in the dust storm cases, but the absolute shape impacts are stronger, up to +9.3 W m^{-2} at the surface.

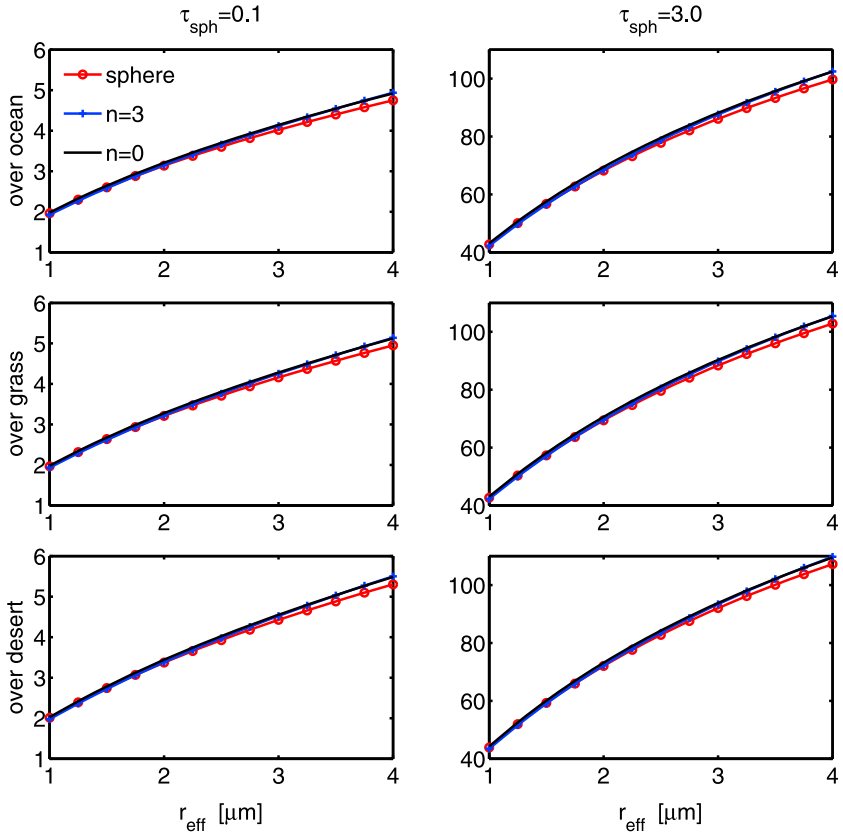

Figure 6. Same as Figure 4 but for diurnally averaged radiative effects of dust on atmospheric absorption (DRE_{ABS}). Units are W m^{-2}.

[27] To visualize the different dependencies of the mass-conserving and τ-conserving cases on r_{eff} and the assumed shape distribution of spheroids, Figure 8 shows the shape impacts at the TOA based on both cases as a function of τ and r_{eff}. The differences are shown only for ocean surface. In both cases, the shape impacts become stronger with increasing τ, but the dependence on r_{eff} is different: in the mass-conserving case the absolute values of shape impacts are largest for the highest values of r_{eff}, while in the τ-conserving case for the smallest r_{eff}. This means that in the mass-conserving case the strongest shape impact is obtained when there are a high number of large dust particles present, while in the τ-conserving case the strongest shape impact occurs when a high number of small dust particles are present. In the τ-conserving case the maximum shape impact obtained over ocean is slightly over 10 W m^{-2} at the TOA and almost 16 W m^{-2} at the surface. The shape impacts are weaker for the mass-conserving case because in that case the larger g and τ of spheroids partly cancel each other's effects.

Table 3. Difference Between the Radiative Effects of Spheroids and Spheres (i.e., the Shape Impact) at the Top of the Atmosphere (TOA) and Surface, as Well as in Atmospheric Absorption (ABS) in the Mass-Conserving Case[a]

	Ocean			Desert		
	TOA	ABS	Surface	TOA	ABS	Surface
τ_{sph} = 0.1						
n = 0	−0.26 (4.8%)	0.04 (1.6%)	−0.30 (3.8%)	−0.14 (9.9%)	0.04 (1.5%)	−0.18 (4.4%)
n = 3	−0.01 (0.2%)	−0.02 (−0.7%)	+0.01(−0.1%)	−0.05 (3.4%)	−0.02 (−0.8%)	−0.03 (0.7%)
τ_{sph} = 0.3						
n = 0	−0.63 (4.4%)	0.12 (1.6%)	−0.75 (3.4%)	−0.38 (9.2%)	0.12 (1.5%)	−0.49 (4.1%)
n = 3	+0.07 (−0.5%)	−0.05 (−0.7%)	+0.12 (−0.5%)	−0.10 (2.3%)	−0.06 (−0.8%)	−0.04 (0.3%)
τ_{sph} = 1.0						
n = 0	−3.14 (12.3%)	1.43 (3.5%)	−4.57 (6.9%)	−1.33 (49.3%)	1.42 (3.1%)	−2.75 (6.4%)
n = 3	−1.59 (6.2%)	1.47 (3.6%)	−3.07 (4.6%)	−0.52 (−19.4%)	1.50 (3.3%)	−2.02 (4.7%)
τ_{sph} = 3.0						
n = 0	−5.05 (10.0%)	2.73 (2.7%)	−7.78 (5.2%)	−2.94 (−53.4%)	2.32 (2.2%)	−5.26 (5.2%)
n = 3	−2.51 (5.0%)	2.75 (2.8%)	−5.27 (3.5%)	−1.26 (−22.8%)	2.54 (2.4%)	−3.79 (3.7%)

[a]Relative shape impacts (in %) and absolute shape impacts (in W m^{-2}) over ocean and desert surfaces are shown for the background (r_{eff} = 1.5 with τ_{sph} = 0.1 and τ_{sph} = 0.3) and dust storm (r_{eff} = 4.0 with τ_{sph} = 1.0 and τ_{sph} = 3.0) cases.

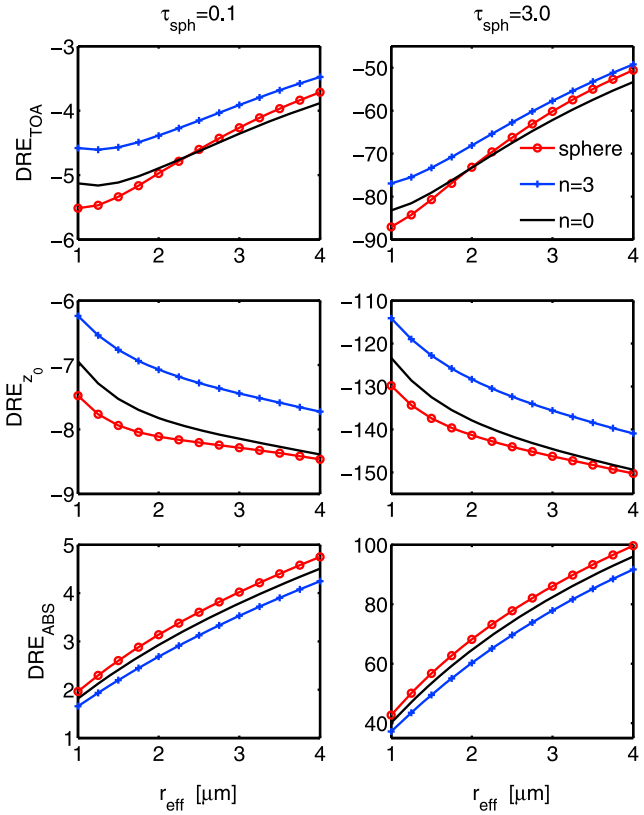

Figure 7. Diurnally averaged direct radiative effects of spherical and spheroidal (τ-conserving case) dust particles at the top of the atmosphere (DRE_{TOA}), at the surface (DRE_{z_0}), and on the atmospheric absorption (DRE_{ABS}). Results with two optical thicknesses (τ_{sph} = 0.1 and τ_{sph} = 3.0) are shown over an ocean surface as a function of r_{eff} in units of W m^{-2}. Values of g and ω are the same as in the mass-conserving case.

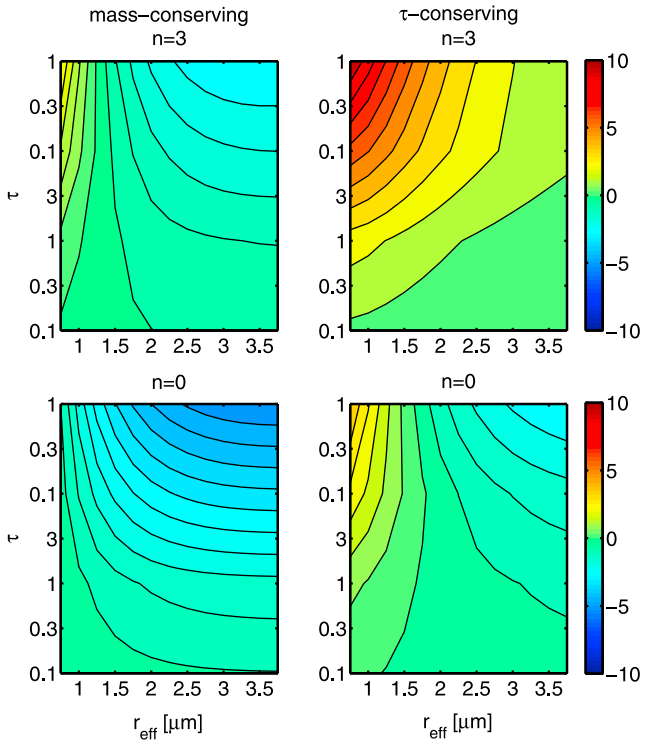

Figure 8. Difference between direct radiative effects of dust at the TOA (W m^{-2}) based on spheroidal (n = 0 and n = 3 distributions) and spherical dust particles i.e., the shape impact over ocean as a function of optical thickness (τ) and effective radius (r_{eff}). Results obtained by using both (left) the mass-conserving and (right) the τ-conserving spheroids are shown.

It is important to notice that, in both cases, the radiative effects based on the studied shape distributions of spheroids may deviate more from each other than from spheres. In addition, the sign of the shape impact can be different depending on the shape distribution and whether the mass or the optical thickness is conserved.

6. Conclusions

[28] In this paper, we have studied the impact of particle nonsphericity on the direct shortwave radiative effects of dust (DRE), by comparing model simulations based on spherical and spheroidal dust particles. It was found that

Table 4. Difference Between the Radiative Effects of Spheroids and Spheres (i.e., the Shape Impact) at the Top of the Atmosphere (TOA) and Surface, as Well as in Atmospheric Absorption (ABS) in the τ-Conserving Case[a]

	Ocean			Desert		
	TOA	ABS	Surface	TOA	ABS	Surface
τ_{sph} = 0.1						
n = 0	+0.22 (−4.2%)	−0.19 (−7.3%)	+0.41 (−5.2%)	−0.00 (0.0%)	−0.21 (−7.5%)	+0.21 (−4.9%)
n = 3	+0.77 (−4.4%)	−0.41 (−15.6%)	+1.17 (−4.8%)	0.18 (−12.3%)	−0.43 (−15.7%)	+0.61 (−4.5%)
τ_{sph} = 0.3						
n = 0	+0.57 (−4.0%)	−0.53 (−7.2%)	+1.10 (−5.0%)	+0.00 (−0.0%)	−0.57 −7.3%)	+0.57 (−4.8%)
n = 3	+2.02 (−4.0%)	−1.13 (−15.3%)	+3.15 (−4.4%)	0.51 (−12.4%)	−1.20 (−15.3%)	+1.71 (−4.3%)
τ_{sph} = 1.0						
n = 0	−1.31 (+5.1%)	−1.82 (−4.4%)	+0.52 (−0.8%)	−1.43 (−52.9%)	−2.11 (−4.6%)	+0.69 (−1.6%)
n = 3	+1.33 (−5.2%)	−3.94 (−9.6%)	+5.27 (−7.9%)	−0.78 (−29.0%)	−4.40 (−9.7%)	+3.62 (−8.5%)
τ_{sph} = 3.0						
n = 0	−2.76 (+5.4%)	−3.64 (−3.7%)	+0.88 (−0.6%)	−3.01 (−54.7%)	−4.06 (−3.8%)	+1.05 (−1.0%)
n = 3	+1.33 (−2.6%)	−7.99 (−8.0%)	+9.31 (−6.2%)	−1.52 (−27.6%)	−8.30 (−7.7%)	+6.78 (−6.7%)

[a]Relative shape impacts (in %) and absolute shape impacts (in W m^{-2}) over ocean and desert surfaces are shown for the background (r_{eff} = 1.5 with τ_{sph} = 0.1 and τ_{sph} = 0.3) and dust storm (r_{eff} = 4.0 with τ_{sph} = 1.0 and τ_{sph} = 3.0) cases.

accounting for dust particles' nonsphericity can make the DRE either larger or smaller depending on the assumed shape distribution of spheroids (n = 3 or n = 0), parameters such as dust optical thickness, surface albedo, and solar zenith angle, and whether the mass or optical thickness is conserved when using spheroids. Moreover, in some cases, two distributions of spheroids may deviate more from each other than either deviates from spheres.

[29] To illustrate the nature of the results from the point of view of aerosol modeling, consider DRE at the surface for the n = 3 distribution of spheroids, which was recently found to reproduce the laboratory measured dust asymmetry parameter better than the n = 0 distribution [*Merikallio et al.*, 2011]. Were one to apply this distribution in an aerosol model that predicts both aerosol mass and number, such as HAM [*Stier et al.* 2005], the mass-conserving case seems like the most logical choice. In that case, the DRE at the surface is quite close to that of spheres, within 5% for the cases we have studied. The small differences are, however, a consequence of compensating nonsphericity effects on optical thickness, asymmetry parameter, and single-scattering albedo. For a given particle mass, spheroids have a larger surface area than spheres, which leads to larger optical thickness and increased negative DRE at the surface. However, the n = 3 distribution also has a larger asymmetry parameter and single-scattering albedo, which acts to reduce the negative DRE at the surface. This compensation is eliminated if the aerosol model is tuned to match satellite observations of optical thickness. In that case the optical thickness conserving case becomes more relevant, and the choice of spheroidal versus spherical particles gains more importance. Then, because of the larger g and ω for the n = 3 distribution, the negative DRE at the surface can be up to 17% smaller than that for spheres. Note also that at the top of the atmosphere, the relative differences between DRE for spheroids and spheres can be greater than those at the surface, especially over high-albedo surfaces.

[30] Overall, the differences between mass- and τ-conserving spheroids, those between the assumed shape distributions of spheroids, and those between spheroids and spheres are roughly equal in magnitude. This makes it difficult to identify any simple pattern in the impact of particle shape on radiative effect. Therefore, although numerous studies show that spheroids can mimic scattering by real dust particles remarkable well, whereas spheres cannot, it is not immediately obvious that using spheroidal dust particles in climate simulations instead of spheres would lead to significantly different results. While we think it would be worth addressing this in a sensitivity study with a climate model, it is likely that the effects are small compared with other uncertainties related to both aerosol modeling and remote sensing [e.g., *Mishchenko et al.*, 1995]. First, in contrast to its moderate effects on radiative fluxes, the effect of dust particle shape on the scattering matrix, including the phase function, is very strong, and can cause errors in the retrieved optical thickness exceeding a factor of 2 or 3 [*Mishchenko et al.*, 2003]. Second, the differences in model predictions of dust optical thickness between existing models are similarly large, if not greater [*Kinne et al.*, 2006].

[31] **Acknowledgments.** Päivi Mauno, Timo Nousiainen, and Petri Räisänen acknowledge funding from the Academy of Finland (contracts 121482, 125180, and 127210), and Michael Kahnert acknowledges funding from the Swedish Research Council (contract 80438701). We also wish to thank O. Dubovik for making his dust optical database available and the anonymous referees for their suggestions.

References

Anderson, G., S. Clough, F. Kneizys, J. Chetwynd, and E. Shettle (1986), AFGL atmospheric constituent profiles (0–120 km), *Tech. Rep. AFGL-TR 86-0110*, Air Force Geophys. Lab., Hanscom Air Force Base, Bedford, Mass.

Baldridge, A. M., S. J. Hook, C. I. Grove, and G. Rivera (2009), The ASTER spectral library version 2.0, *Remote Sens. Environ.*, *113*, 711–715, doi:10.1016/j.rse.2008.11.007.

Dubovik, O., B. Holben, T. F. Eck, A. Smirnov, Y. J. Kaufman, M. D. King, D. Tanré, and I. Slutsker (2002), Variability of absorption and optical properties of key aerosol types observed in worldwide locations, *J. Atmos. Sci.*, *59*, 590–608, doi:10.1175/1520-0469(2002)059<0590:VOAAOP>2.0.CO;2.

Dubovik, O., et al. (2006), Application of spheroids models to account for aerosol particle nonsphericity in remote sensing of desert dust, *J. Geophys. Res.*, *111*, D11208, doi:10.1029/2005JD006619.

Kahnert, M., and A. Kylling (2004), Radiance and flux simulations for mineral dust aerosols: Assessing the error due to using spherical or spheroidal model particles, *J. Geophys. Res.*, *109*, D09203, doi:10.1029/2003JD004318.

Kahnert, M., and T. Nousiainen (2006), Uncertainties in measured and modelled asymmetry parameters of mineral dust aerosols, *J. Quant. Spectrosc. Radiat. Transfer*, *100*, 173–178, doi:10.1016/j.jqsrt.2005.11.035.

Kahnert, M., and T. Rother (2011), Modeling optical properties of particles with small-scale surface roughness: Combination of group theory with a perturbation approach, *Opt. Express*, *19*, 11,138–11,151, doi:10.1364/OE.19.011138.

Kahnert, M., J. J. Stamnes, and K. Stamnes (2002), Can simple particle shapes be used to model scalar optical properties of an ensemble of wavelength-sized particles with complex shapes?, *J. Opt. Soc. Am. A Opt. Image Sci. Vis.*, *19*, 521–531, doi:10.1364/JOSAA.19.000521.

Kahnert, M., T. Nousiainen, and B. Veihelmann (2005), Spherical and spheroidal model particles as an error source in aerosol climate forcing and radiance computations: A case study for feldspar aerosols, *J. Geophys. Res.*, *110*, D18S13, doi:10.1029/2004JD005558.

Kahnert, M., T. Nousiainen, and P. Räisänen (2007), Mie simulations as an error source in mineral aerosol radiative forcing calculations, *Q. J. R. Meteorol. Soc.*, *133*, 299–307, doi:10.1002/qj.40.

Kahnert, M., et al. (2012), Light scattering by particles with small-scale surface roughness: Comparison of four classes of model geometries, *J. Quant. Spectrosc. Radiat. Transfer*, in press.

Kalashnikova, O. V. K., R. Kahn, I. N. Sokolik, and W.-H. Li (2005), Ability of multiangle remote sensing observations to identify and distinguish mineral dust types: Optical models and retrieval of optically thick plumes, *J. Geophys. Res.*, *110*, D18S14, doi:10.1029/2004JD004550.

Kato, S., T. P. Ackerman, J. H. Mather, and E. Clothiaux (1999), The *k*-distribution method and correlated-*k* approximation for a shortwave radiative transfer model, *J. Quant. Spectrosc. Radiat. Transfer*, *62*, 109–121, doi:10.1016/S0022-4073(98)00075-2.

Kinne, S., et al. (2003), Monthly averages of aerosol properties: A global comparison among models, satellite data, and AERONET ground data, *J. Geophys. Res.*, *108*(D20), 4634, doi:10.1029/2001JD001253.

Kinne, S., et al. (2006), An AeroCom initial assessment—Optical properties in aerosol component modules of global models, *Atmos. Chem. Phys.*, *6*, 1815–1834, doi:10.5194/acp-6-1815-2006.

Mayer, B., and A. Kylling (2005), Technical note: The libRadtran software package for radiative transfer calculations–Description and examples of use, *Atmos. Chem. Phys.*, *5*, 1855–1877, doi:10.5194/acp-5-1855-2005.

Merikallio, S., H. Lindqvist, T. Nousiainen, and M. Kahnert (2011), Modeling light scattering by mineral dust using spheroids: Assessment of applicability, *Atmos. Chem. Phys.*, *11*, 5347–5363, doi:10.5194/acp-11-5347-2011.

Middleton, N. J., P. R. Betzer, and P. A. Bull (2001), Long-range transport of 'giant' aeolian quarts grains: Linkage with discrete sedimentary sources and implications for protective particle transfer, *Mar. Geol.*, *177*, 411–417, doi:10.1016/S0025-3227(01)00171-2.

Mishchenko, M. I., and L. D. Travis (1994), *T-matrix* computations of light scattering by large spheroidal particles, *Opt. Commun.*, *109*, 16–21, doi:10.1016/0030-4018(94)90731-5.

Mishchenko, M. I., A. A. Lacis, B. E. Carlson, and L. D. Travis (1995), Nonsphericity of dust-like tropospheric aerosols: Implications for aerosol remote sensing and climate modelling, *Geophys. Res. Lett.*, *22*, 1077–1080, doi:10.1029/95GL00798.

Mishchenko, M. I., L. D. Travis, and A. Macke (1996), Scattering of light by polydisperse, randomly oriented, finite circular cylinders, *Appl. Opt.*, *35*, 4927–4940, doi:10.1364/AO.35.004927.

Mishchenko, M. I., L. D. Travis, R. A. Kahn, and R. A. West (1997), Modeling phase functions for dustlike tropospheric aerosols using a shape

mixture of randomly oriented polydisperse spheroids, *J. Geophys. Res.*, *102*, 16,831–16,847, doi:10.1029/96JD02110.

Mishchenko, M. I., I. V. Geogdzhayev, L. Liu, J. A. Ogren, A. A. Lacis, W. B. Rossow, J. W. Hovenier, H. Volten, and O. Muñoz (2003), Aerosol retrievals from AVHRR radiances: Effects of particle nonsphericity and absorption and an updated long-term global climatology of aerosol properties, *J. Quant. Spectrosc. Radiat. Transfer*, *79–80*, 953–972, doi:10.1016/S0022-4073(02)00331-X.

Mishchenko, M. I., J. M. Dlugach, and D. W. Mackowski (2011) Light scattering by wavelength-sized particles "dusted" with subwavelength-sized grains, *Opt. Lett.*, *36*, 337–339.

Myhre, G., and F. Stordal (2001), Global sensitivity experiment of the radiative forcing due to mineral aerosols, *J. Geophys. Res.*, *106*, 18,193–18,204, doi:10.1029/2000JD900536.

Nousiainen, T. (2009), Optical modeling of mineral dust particles: A review, *J. Quant. Spectrosc. Radiat. Transfer*, *110*, 1261–1279, doi:10.1016/j.jqsrt.2009.03.002.

Nousiainen, T., and K. Vermeulen (2003), Comparison of measured single-scattering matrix of feldspar particles with *T*-matrix simulations using spheroids, *J. Quant. Spectrosc. Radiat. Transfer*, *79–80*, 1031–1041.

Nousiainen T., M. Kahnert, and B. Veihelmann (2006), Light scattering modeling of small feldspar aerosol particles using polyhedral prism and spheroids, *J. Quant. Spectrosc. Radiat. Transfer*, *101*, 471–487, doi:10.1016/j.jqsrt.2006.02.038.

Nousiainen, T., M. Kahnert, and H. Lindqvist (2011), Can particle shape information be retrieved from light scattering observations using spheroidal model particles?, *J. Quant. Spectrosc. Radiat. Transfer*, *112*, 2213–2225, doi:10.1016/j.jqsrt.2011.05.008.

Otto S., T. Trautmann, and M. Wendisch (2011), On realistic size equivalence and shape of spheroidal Saharan mineral dust particles applied in solar and thermal radiative transfer calculations, *Atmos. Chem. Phys.*, *11*, 4469–4490.

Ramanathan, V., P. J. Crutzen, J. T. Kiehl, and D. Rosenfeld (2001), Aerosols, climate, and the hydrological cycle, *Science*, *294*, 2119–2124, doi:10.1126/science.1064034.

Roeckner, E., et al. (2003), The atmospheric general circulation model ECHAM5. Part I: Model description, *Rep. 439*, Max Planck Inst. for Meteorol., Hamburg, Germany.

Sokolik, I. N., and O. B. Toon (1996), Direct radiative forcing by anthropogenic airborne mineral aerosols, *Nature*, *381*, 681–683, doi:10.1038/381681a0.

Sokolik, I. N., and O. B. Toon (1999), Incorporation of mineralogical composition into models of the radiative properties of mineral aerosol from UV to IR wavelengths, *J. Geophys. Res.*, *104*, 9423–9444, doi:10.1029/1998JD200048.

Stamnes, K., S. Tsay, W. Wiscombe, and K. Jayaweera (1988), A numerically stable algorithm for discrete-ordinate-method radiative transfer in multiple scattering and emitting layered media, *Appl. Opt.*, *27*, 2502–2509, doi:10.1364/AO.27.002502.

Stier, P., et al. (2005), The aerosol-climate model ECHAM5-HAM, *Atmos. Chem. Phys.*, *5*, 1125–1156, doi:10.5194/acp-5-1125-2005.

Volten, H., O. Muñoz, E. Rol, J. F. de Haan, W. Vassen, J. W. Hovenier, K. Muinonen, and T. Nousiainen (2001), Scattering matrices of mineral aerosol particles at 441.6 and 632.8 nm, *J. Geophys. Res.*, *106*(D15), 17,375–17,401, doi:10.1029/2001JD900068.

Wiegner, M., et al. (2009), Numerical simulations of optical properties of Saharan dust aerosols with emphasis on lidar applications, *Tellus, Ser. B*, *61*, 180–194, doi:10.1111/j.1600-0889.2008.00381.x.

Yang, P., and K. N. Liou (1996), Geometric-optics-integral-equation method for light scattering by nonspherical ice crystals, *Appl. Opt.*, *35*, 6568–6584, doi:10.1364/AO.35.006568.

Yang, P., Q. Feng, G. Hong, G. W. Kattawar, W. J. Wiscombe, M. I. Mishchenko, O. Dubovik, I. Laszlo, and I. N. Sokolik (2007), Modeling of the scattering and radiative properties of nonspherical dust-like aerosols, *J. Aerosol Sci.*, *38*, 995–1014, doi:10.1016/j.jaerosci.2007.07.001.

P. Haapanala and T. Nousiainen, Department of Physics, University of Helsinki, PO Box 48, FI-00014 Helsinki, Finland. (paivi.mauno@helsinki.fi)

M. Kahnert, Research Department, Swedish Meteorological and Hydrological Institute, Folkborgsvägen 1, S-60176 Norrköping, Sweden.

P. Räisänen, Climate Change Research, Finnish Meteorological Institute, PO Box 503, FI-00101 Helsinki, Finland.